
Article:
Barton, D.N.T., Robshaw, T.J., Okusanya, O. et al. (5 more authors) (2019) Remediation of radioiodine using polyamine anion exchange resins. Journal of Industrial and Engineering Chemistry, 78. pp. 210-221. ISSN 1226-086X

https://doi.org/10.1016/j.jiec.2019.06.012

Remediation of Radioiodine Using Polyamine Anion Exchange Resins

Daniel N. T. Barton[1], Thomas J. Robshaw*[1], Oluwatobi Okusanya[1], Daigeun Kim[2], Sarah E. Pepper[1], Clint A. Sharrad[3], Taek Seung Lee[2], Mark D. Ogden[1]

*Corresponding author: tjrobshaw1@sheffield.ac.uk

[1]Separations and Nuclear Chemical Engineering Research, Department of Chemical and Biological Engineering, The University of Sheffield, Sheffield S1 3JD, United Kingdom

[2]Department of Organic Materials Engineering, Chungnam National University, Daejeon, Republic of Korea

[3]School of Chemical Engineering and Analytical Science, The University of Manchester, Oxford Road, Manchester M13 9PL, United Kingdom.

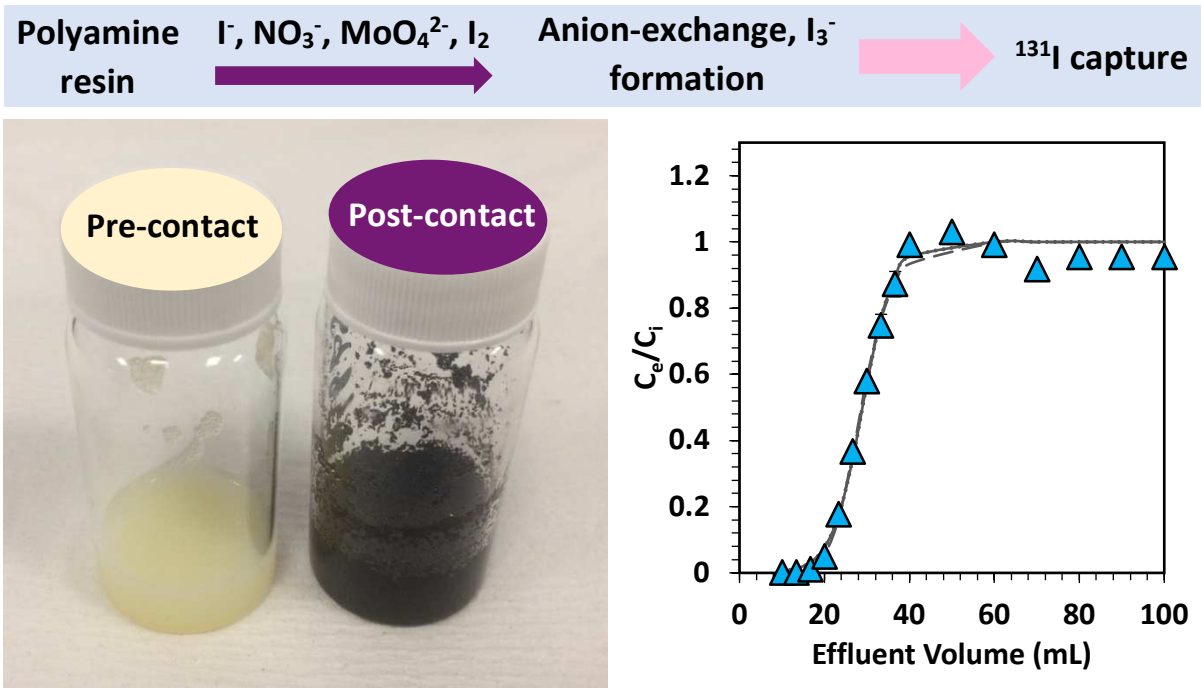

Two weak base anion exchange resins, Lewatit A365 and Purolite MTS9850, have been tested for the removal of aqueous iodide from conditions simulating nuclear waste reprocessing streams. pH variation and relevant co-contaminant addition (nitrate, molybdate and iodine) allowed for assessment of iodide extraction behaviour of each resin. Isotherm experiments were performed and maximum uptake capacities obtained exceed current industrial adsorbents, such as silver-impregnated zeolites. Maximum loading capacities, determined by Dubinin-Radushkevich isotherm,

were 761 ± 14 mg g^{-1} for MTS9850 and 589 ± 15 mg g^{-1} for A365. Uptake for both resins was significantly suppressed by nitrate and molybdate ions. The presence of dissolved iodine in the raffinate however, was found to increase iodide uptake. This was explained by characterisation of the spent resin surface by infrared and Raman spectroscopy, which determined the presence of triiodide, indicating charge-transfer complex formation on the surface. Dynamic studies assessed the effect of co-contaminants on iodide uptake in a column environment. Data was fitted to three dynamic models, with the Dose-Response model providing the best description of breakthrough. In all cases iodide breakthrough was accelerated, indicating suppression of uptake, but capacity was still significant.

Keywords: anion exchange, radioiodine, Purolite MTS9850, Lewatit A365, remediation

- Weak-base polyamine resins have demonstrated very large iodide uptake capacities.
- Dubinin-Radushkevich isotherm-fitting confirms an anion-exchange mechanism is prevalent.
- Breakthrough behaviour is well-described by the Dose-Response model.
- Co-existing anions molybdate and nitrate suppressed uptake, but not completely.
- Addition of diiodine increased uptake, seemingly due to charge-transfer complex formation with the resin matrix.

1. Introduction

The fission of uranium-235 produces a variety of isotopes of various elements, from zinc through to the lanthanides. Four isotopes of iodine are produced in the fission process with significant yields [1]. Of these, iodine-129 (^{129}I) and iodine-131 (^{131}I) are a concern due to their ability to damage human health and the environment. Iodine displays a capricious chemistry which includes a variety of oxidation states, formation of organic compounds, and volatility. This diversity in chemical behaviour makes iodine challenging to capture, remove and immobilize from nuclear waste streams [2]. ^{129}I has an extremely long half-life ($t_{1/2}$ = 15.7 million years), whilst ^{131}I has a short half-life ($t_{1/2}$ = 8.02 days), yet both have high mobility within the environment [1, 3]. ^{131}I poses a severe risk to human health, particularly small children, due to high specific activity and ability to accumulate in the thyroid gland [4]. Conveniently, its short half-life results in little to no impact on nuclear waste disposal [5]. The long half-life of ^{129}I is more of a concern for long-term waste storage in a geological repository. It is consistently found to be one of the largest radioactivity dose contributors in the assessment of such repositories [6]. Aqueous radioiodine has also been shown to bio-accumulate in aquatic ecosystems [7], which can potentially result in human uptake and exposure.

During power generation, iodine can leach into coolant systems of the plant through fission product pathways, as a result of cladding or fuel handling failures [8]. In the processing of used nuclear fuel (UNF), iodine partitions between a variety of gaseous streams and aqueous phases, leading to the potential for release at every stage of unit operation. Iodine most readily escapes as an off-gas, with a small fraction remaining within the aqueous raffinate [9]. There are a number of commonly applied methods to limit the volume of iodine emissions, to remain in line with regulations. For example, ^{129}I is often removed using caustic scrubbing or via adsorption using silver-impregnated silica or zeolites, whilst ^{131}I removal involves acidic scrubbing processes [10]. Major challenges arise when considering the removal of the remaining iodine present in liquid waste streams and subsequently how the volume of aqueous iodine discharge can be more effectively reduced.

In an acidic environment, iodide is known to be the dominant species of aqueous iodine [11]. With this knowledge in mind, a potential solution can be outlined. A promising option is ion-exchange, which has been widely used within the nuclear industry, most commonly for coolant purification and similar processes, such as condensate polishing [12]. There has however been minimal research into the removal of volatile fission products, such as iodine, from aqueous waste streams. Current solid sorbents such as activated charcoal and zeolites have poor uptake capacities in these challenging environments and often high raw material costs, particularly if impregnated with metals such as silver [13, 14]. Ion-exchange resins are an economically preferable choice and have been shown to display greater iodide uptake than industrially implemented methods [8, 15].

In this study, two weak-base anion (WBA) resins have been compared under a variety of conditions, approximately simulating UNF reprocessing aqueous waste streams, with the aim of determining uptake capacities for iodide anions. Anion-exchange resins are available in strong base and weak base forms, allowing for applications in a wide range of environments. WBAs are predicted to be more effective for iodide removal due to their increased selectivity and uptake capacities for larger anions compared to strong base resins. Their optimum operating pH range also ensures suitability for operation in the strongly acidic conditions present [16].

The two commercially available resins, Purolite MTS9850 and Lewatit A365, have recommended applications for water purification and heavy metal removal, notably platinum, palladium and rhodium. However, there is minimal literature data available with respect for their suitability for the targeted removal of anions, and none at all for iodide specifically. Predominantly, research carried out using Purolite MTS9850 has focused on the removal of specific transition metals [17 - 19], while Lewatit A365 has had one sole literature publication, targeting uranium recovery from various media [20]. This makes it difficult to predict the relative uptake capacities and affinities of these tested resins for iodide.

This work represents one of the first attempts to study removal of iodine from aqueous nuclear waste streams by iodide ion-exchange, as well as comparing the performance of two WBA resins of little previous documentation. It will also begin to address the issue of the adverse effects of co-existing anions on iodide uptake. Furthermore, the effect of introducing molecular iodine into an iodide system, and subsequently forming equilibrium with triiodide ion has not previously been documented to our knowledge. Overall, the suitability of each resin for iodide uptake in the nuclear industry will be assessed, with the potential for further kinetic studies and scale-up operation to be carried out.

2. Experimental

2.1. Reagents and stock solutions

All reagents were supplied by commercial suppliers Sigma Aldrich and Acros Organics, at analytical grade or higher, and were used as received. The majority of reagents were purchased as sodium salts (NaI, $NaNO_3$, $Na_2MoO_4.2H_2O$), used to simulate ions that are present in nuclear waste reprocessing streams. Elemental iodine in its solid form was also used for this reason, as well as to aid in the understanding of how it behaves in the presence of ion-exchange resins.

A Cole-Parmer combination iodide ion-selective electrode (epoxy type) was used to carry out ion-selective electrode (ISE) analysis. Calibration was completed by analysing a number of iodide standards across an appropriate range, made from a 1000 mg L^{-1} iodide standard solution (Fisher Scientific). Calibration was performed prior to every new study and after every run of $\leq$10 sample within an experiment, if applicable. All samples included 2% 5 M $NaNO_3$ ionic strength adjuster and were made up to a convenient final volume with deionised water. Each sample was analysed in triplicate. Commercial anion exchange resins Purolite MTS9850 and Lewatit A365 were kindly donated by Purolite and Lanxess respectively. The functionalities of the two resins are shown in Figure 1 and an overview of resin parameters is found in Table 1.

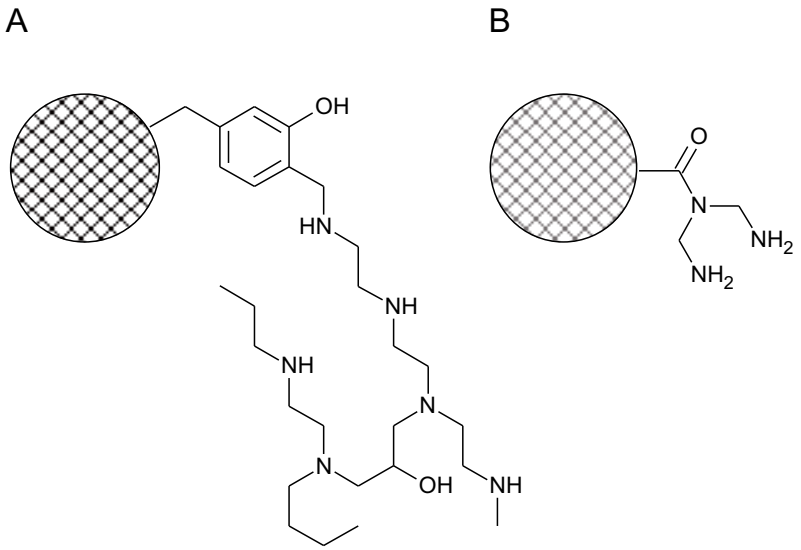

Figure 1. Functionalities of the two WBA resins. A) Purolite MTS9850 and B) Lewatit A365. Shaded circles represent the polymer matrix (acrylate/divinylbenzene).

Table 1. Manufacturer specifications for Purolite MTS9850 and Lewatit A365 (DVB = divinylbenzene).

Parameter	Purolite MTS9850	Lewatit A365
Capacity (eq L^{-1})	2.3	3.4
Moisture content	52-57%	44-51%
Resin bead diameter (mm)	0.3 – 1.2	0.4 – 1.6
Functionality	Polyamine	Polyamine
Type	Weak base/Chelating	Weak base/Chelating
Matrix	Polyacrylic/DVB	Polyacrylic/DVB

Where necessary, pH adjustments were made using solutions of 0.01 – 1 M HNO_3 and NaOH. Preconditioning of the resin was carried out by contacting 150 g of each resin (mass as-received) in 2 L of 1 M HNO_3 for 24 hours at room temperature on an orbital shaker. The preconditioned resin was then subsequently washed with 10 x 2 L of deionised water. An accurate conversion between wet settled volume and dry mass was determined by drying an appropriate volume of preconditioned resin in an air-flow oven at 50°C for a minimum of 24 hours, then recording the change in mass. Five repeat measurements were made and the results averaged.

2.2. Uptake studies – pH and co-contaminants

Varying pH studies were carried out in duplicate, using a solution of 10 g L^{-1} iodide. The pH range tested was 2 – 10 to observe the variation of uptake behaviour over acidic and basic conditions. 25 mL of iodide solution was added to 600 mg of resin (dry mass) and subsequently pH adjusted, using solutions of 0.01 – 1 M HNO_3 and NaOH. The solution was then made up to close to 50 mL with deionised water, with pH being further adjusted as necessary until stable, before samples were made up the final volume and placed on an orbital shaker for 12 hours to achieve equilibrium, prior to ISE analysis. Iodide uptake capacity, q_e (mg g^{-1}), was determined using Eq. (1),

$$q_e = \frac{(C_i - C_e) \times V}{W} \quad (1)$$

where C_i is the initial iodide concentration (mg L^{-1}), C_e is the iodide concentration of the solution at equilibrium (mg L^{-1}), V is volume of the solution analysed (L) and W is mass of resin (g).

The effect of co-contaminants on iodide uptake was studied by addition of sodium nitrate, sodium molybdate and iodine, at concentrations of 1 – 10 g L^{-1}, to 50 mL of 7 g L^{-1} iodide solution, contacted with 600 mg of resin (dry mass). Experiments were carried out at pH ~3 and not adjusted, following initial contact. The samples were placed on an orbital shaker for a minimum of 12 hours and subsequently analysed via ISE and uptake capacity quantified, as per the pH study.

2.3. Isotherm studies

Isotherm experiments were completed in duplicate for Purolite MTS9850 and Lewatit A365, varying initial iodide concentration over a range of 1 – 10 g L^{-1} at one gram intervals. 20 ml solutions were contacted with 250 mg of resin (dry mass) for a minimum of 12 hours and allowed to equilibrate at ambient temperature on an orbital shaker. Experiments were again carried out at pH ~3 and not adjusted, following initial contact. Iodide uptake capacity for each concentration was determined via ISE, as previously described.

Numerous isotherm models can be considered for modelling of uptake behaviour, ranging from one- to five-parameter models [21]. Commonly used two-parameter isotherms have been applied to the data, these being Langmuir, Freundlich, Temkin and Dubinin-Radushkevich [22], for literature comparison on iodide uptake. Data fitting was carried out using linear regression and by non-linear least squares analysis using SOLVER in Microsoft Excel to obtain the best possible fit [23] and standard errors were calculated at 95% confidence intervals.

The Langmuir isotherm model, (Eq. (2)) can be applied to systems with a finite number of adsorption sites. Given that there are a finite number of protonated tertiary amine groups present for both ion exchange resins, the Langmuir model should be applicable.

$$q_e = \frac{K_L C_e}{1 + a_L C_e} \quad (2)$$

In the Langmuir equation, a_L and K_L are Langmuir Isotherm constants. The theoretical maximum possible uptake capacity, q_{max} (mg g^{-1}), can be determined using these constants, as shown by Eq. (3).

$$q_{max} = \frac{K_L}{a_L} \quad (3)$$

However, since the amine environments, particularly for MTS9850, would not be expected to be degenerate (Figure 1), iodide uptake behaviour could also be described by the Freundlich isotherm model [24] (Eq. (4)),

$$q_e = K_F C_e^{\frac{1}{n}} \quad (4)$$

where K_F and n are Freundlich isotherm constants. K_F is a measure of adsorption capacity and n is a factor of heterogeneity [25].

The Temkin isotherm model, (Eq. (5)), has been applied to confirm that heat of adsorption decreases linearly as exchange sites are occupied, as a result of interactions between the solution and the resin [26],

$$q_e = \frac{RT}{b_T} \ln (A_T C_e) \quad (5)$$

where $\frac{RT}{b_T}$ can be represented as B (heat of adsorption constant).

R is the ideal gas constant (8.314 J K^{-1} mol^{-1}), T is temperature (K), while A_T and b_T are Temkin isotherm constants.

The Dubinin-Radushkevich (D-R) model, (Eq. (6)), is used to determine which adsorption mechanism dominates within the system; either chemisorption, ion-exchange or physisorption [27],

$$q_e = q_{max} e^{-B_D \varepsilon^2} \quad (6)$$

where B_D is a D-R isotherm constant (mol^2 J^2) and ε^2 is the Polanyi potential which is described by Eq. (7).

$$\varepsilon^2 = RTln(1 + \frac{1}{C_e}) \quad (7)$$

Mean free energy of sorption E_D (J mol^{-1}) can thus be obtained, which can help to determine which mechanism of adsorption is present and is represented by Eq. (8).

$$E_D = \frac{1}{\sqrt{2B_D}} \quad (8)$$

2.4. Dynamic studies

Wet settled resin (4 mL) was packed into a 5 mL column and a 5 g L^{-1} iodide solution was passed through at a flow rate of 5.25 BV hr^{-1} (BV = bed volumes, the equivalent volume of water to that of the wet settled resin within the column). Tygon tubing with internal diameter of 0.8 mm was used, connected to a Fisher Scientific CTP100 peristaltic pump operating at 10 rpm. Samples were collected with a fraction collector at 15-minute intervals, until full breakthrough was achieved. ISE analysis was carried out as previously described.

The above method was repeated to observe the effect of co-contaminants in a dynamic environment. Once again, these included sodium nitrate, sodium molybdate and iodine, all at 5 g L^{-1} in the inlet solution of their respective experiments. Results were plotted using three common dynamic breakthrough models, these being Dose-Response, Yoon-Nelson and Thomas.

The Dose-Response model (Eq. (9)) is often applied due to the fact it minimises errors produced in other models.

$$\frac{C}{C_i} = 1 - \frac{1}{1+\left(\frac{V_{ef}}{b}\right)^a} \quad (9)$$

In the Dose-Response model, C is the concentration at a specific time (mg L^{-1}), C_i is the initial concentration (mg L^{-1}), V_{ef} is volume of the liquid (mL), whilst a and b are Dose-Response constants.

The Thomas model (Eq. (10)) aims to determine whether adsorption is controlled by interfacial mass transfer, rather than via a chemical reaction.

$$\ln\left(\frac{C_i}{C} - 1\right) = \left(\frac{k_{Th}}{Q}\right)(q_o m) - \left(\frac{k_{Th}}{Q}\right)(C_i V_{ef}) \quad (10)$$

In the Thomas model, k_{Th} is the Thomas rate constant (ml min^{-1} mg^{-1}), Q is flow rate (ml min^{-1}), q_o is maximum uptake capacity (mg g^{-1}) and m is mass of resin (g). All other parameters are as previously described.

The linearized Yoon-Nelson model (Eq. (11)) is the final model to consider, which aids in the prediction of adsorption performance, making a number of assumptions linked to proportionality.

$$\ln\left(\frac{C}{C_i - C}\right) = k_{YN}t - k_{YN}\tau \quad (11)$$

In the Yoon-Nelson model, k_{YN} is the Yoon-Nelson constant (min^{-1}) and τ is the 50% adsorbate breakthrough time constant (min). All other parameters are as previously described.

2.5 Resin characterization

Fourier-transform infrared spectroscopy (FTIR) was carried out using a PerkinElmer Spectrum 2000 ATR FTIR spectrometer. Samples were prepared by grinding the resins, at various process stages, with a small volume of deionised water to produce a fine slurry, before drying in an air-flow oven at 50°C for a minimum of 24 hours. Raman spectroscopy was carried out with a Horiba XploRA Plus microscope, with samples being prepared using the same method. Elemental analysis was performed using a Vario MICRO Cube analyser. 100 mg of each resin was preconditioned with 20 ml of 3 M hydrochloric acid, in order to give accurate nitrogen mass % results. Post-preconditioning, the resins were washed with 50 ml of deionised water and dried for 24 hours at 50 °C.

3. Results

3.1. Effect of pH and co-contaminants on iodide uptake

Iodide uptake of both resins over a pH range from 2 – 10 is shown in Figure 2, which indicates that between pH 2 - 4 uptake remains similar. A 2nd order polynomial fit of the data suggests that optimum extraction can be achieved around pH 3.1 ± 0.01 for both resins. Therefore, all subsequent experiments were run at pH 3, which was very close to the natural pH of NaI solution. Under these conditions, the establishment of equilibrium for the uptake process was observed to not change the solution pH significantly, so no adjustment was performed during the experiments.

The effect of nitrate, molybdate and iodine co-contaminants, which would be present in UNF reprocessing streams, on uptake of iodide by the resins, is presented in Figure 3.

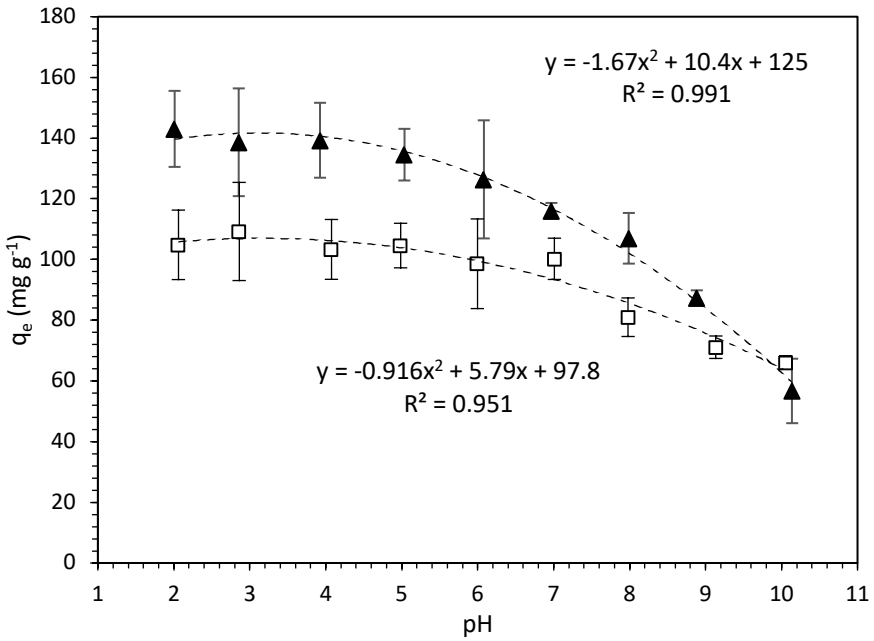

Figure 2. Iodide uptake for ▲ = MTS9850 and □ = A365 across the pH range 2 - 10, adjusted with HNO_3 and NaOH. Solution volume = 25 mL. I^- C_i = 10 g L^{-1}. Equilibration time = 24 hours. Resin mass = 600 mg. T = 20°C. Error bars show 95% confidence intervals. Data points represent equilibrium pH of each solution. 2nd order polynomial fit of the data points is used to guide the eye.

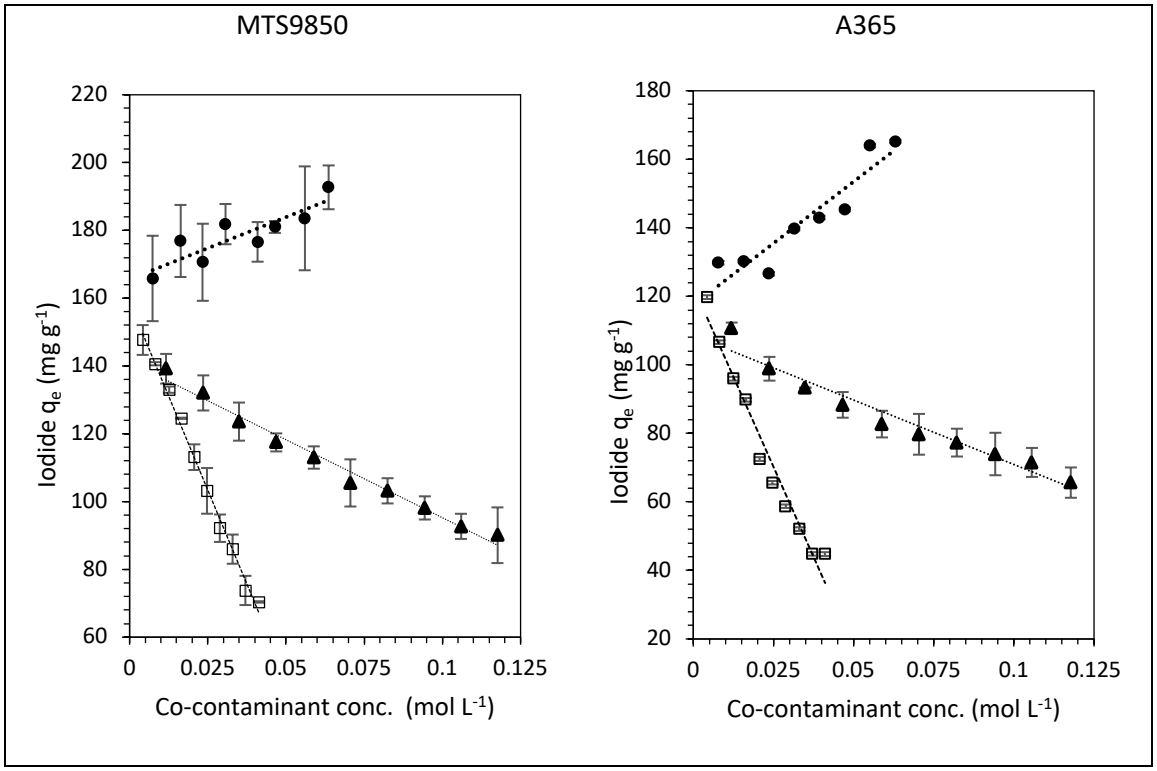

Figure 3. Variation of iodide uptake capacity with the introduction of ▲ = nitrate, □ = molybdate and ● = iodine at concentrations of 1 - 10 g L^{-1}. Equilibration time = 24 hours. Solution volume = 25 mL. I^- C_i = 10 g L^{-1}. Resin mass = 600 mg. T = 20°C. pH = 3. Best fit lines are displayed to show linear relationships between co-contaminant concentration and suppression of iodide uptake.

3.2. Isotherms

Figure 4 shows isotherms for Purolite MTS9850 and Lewatit A365 respectively across a fixed range of starting concentrations and includes fits to the two-parameter models. Relevant parameters for each model were extracted and are presented in Table 2.

The Langmuir separation factor, R_L was calculated from Eq. (15) [28].

$$R_L = \frac{1}{1+K_L C_i} \quad (15)$$

This value determines how favourable the adsorption is onto the resin, with a value approaching 0 representing very strong adsorption.

For an arbitrary iodide concentration of 5 g L^{-1}, MTS9850 demonstrates a slightly stronger adsorption than A365 – a value of 2.5 x 10^{-4} compared to 9.4 x 10^{-4}.

The D-R model provided the highest R^2 value for the attained data (Table 2) and therefore the derived q_D values were considered the most valid for estimating the maximum iodide adsorption capacity of the resins.

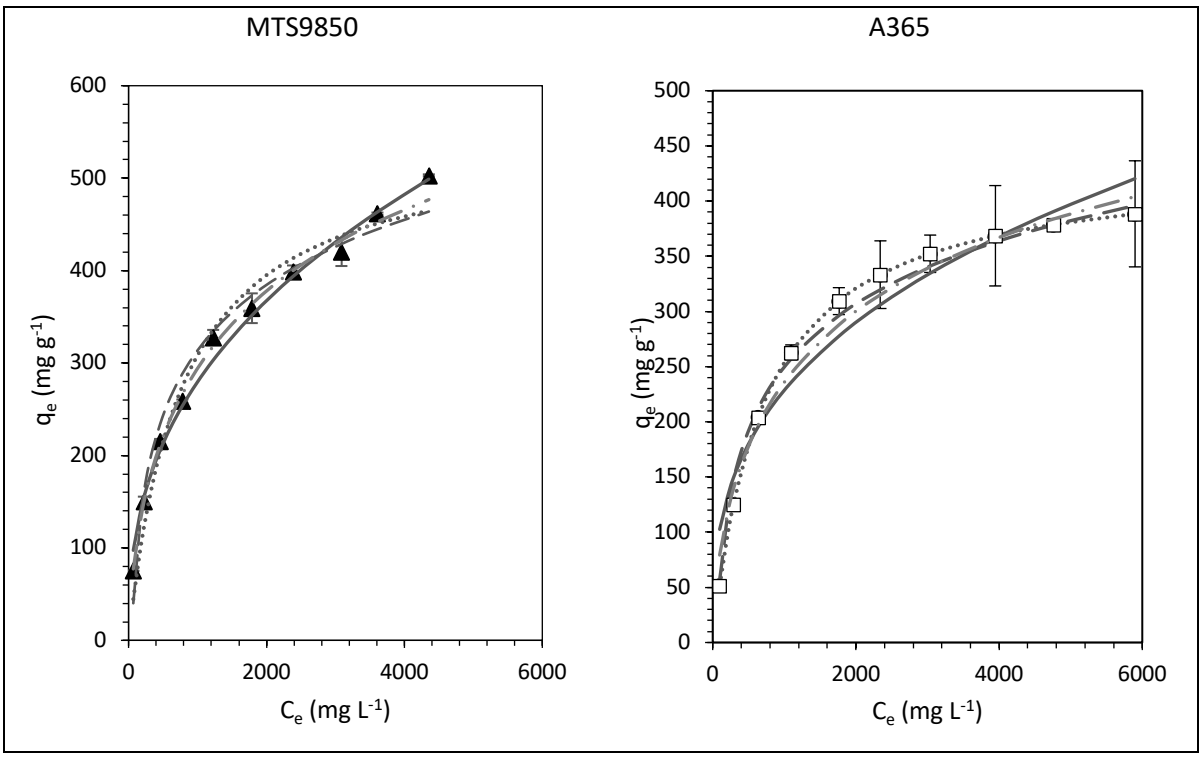

Figure 4. Isotherm uptake of iodide by ▲ = Purolite MTS9850 and □ = Lewatit A365 for C_i range 1000 – 10000 mg L^{-1}. Equilibration time = 24 hours. Solution volume = 20 mL. Resin mass = 250 mg. T = 20°C. pH = 3. Error bars show 95% confidence intervals. Models used to fit are indicated by lines on the graph; solid grey line = Freundlich, grey dotted line = Langmuir, grey dashed line = Temkin, grey dashed-dotted line = D-R.

Table 2. Key parameters obtained from fitting experimental data to the Langmuir, Freundlich, Temkin and D-R isotherm models for a fixed concentration range between 1000 – 10000 mg L^{-1}.

Model	Parameter	Purolite MTS9850	Lewatit A365
Langmuir	K_L	0.75 ± 0.02	0.604 ± 0.003
	a_L (g mg^{-1})	1.37 ± 0.05 (x 10^{-3})	1.39 ± 0.06 (x 10^{-3})
	q_{max} (mg g^{-1})	549 ± 2	440 ± 20
	R^2	0.982	0.991
Freundlich	K_F (mg g^{-1})	18.5 ± 0.8	21.3 ± 0.4
	n	2.54 ± 0.04	2.91 ± 0.05
	R^2	0.990	0.973
Temkin	A_T (L g^{-1})	2.20 ± 0.20 (x 10^{-2})	2.05 ± 0.08 (x 10^{-2})
	b_T	24.4 ± 0.4	30 ± 1
	B (J mol^{-1})	101 ± 2	83 ± 3
	R^2	0.968	0.984
Dubinin-Radushkevich	B_D (mol^2 J^{-2})	6.76 ± 0.35 (x 10^{-9})	6.51 ± 0.37 (x 10^{-9})
	q_D	761 ± 14	589 ± 15
	E_D (kJ mol^{-1})	8.60 ± 0.19	8.76 ± 0.21
	R^2	0.999	0.999

3.3. Fixed-bed dynamic studies

Through observations from all previous experiments, Purolite MTS9850 demonstrated superior iodide uptake capacity in relevant experimental conditions. Therefore, this resin was carried forward to look at column experiments. The breakthrough behaviour of the column with various co-contaminants is shown in Figures 5 and 6. Table 3 provides the extracted key parameters for each model from the breakthrough data.

Table 3. Key parameters for dynamic models used to fit the experimental breakthrough values.

Model	Parameter	Iodide	Iodide + NO_3^-	Iodide + MoO_4^{2-}	Iodide + I_2	Iodide + all
Thomas	k_{TH} (ml min^{-1} mg^{-1})	2.70 x 10^{-3}	6.36 x 10^{-3}	5.89 x 10^{-3}	3.32 x 10^{-3}	9.14 x 10^{-3}
	q_o (mg g^{-1})	230	111	137	152	69.9
	R^2	0.864	0.999	0.991	0.964	0.970
Yoon-Nelson	k_{YN} (min^{-1})	8.02 x 10^{-3}	0.0309	0.0401	9.53 x 10^{-3}	0.0462
	τ (min)	605	270	276	692	174
	R^2	0.975	0.999	0.991	0.964	0.970
Dose-Response	a	4.301	8.34	5.13	7.06	7.92
	b	207	93.6	65.5	136.1	28.7
	q_0 (mg g^{-1})	278	110	161	149	69.2
	R^2	0.987	0.999	0.899	0.961	0.971

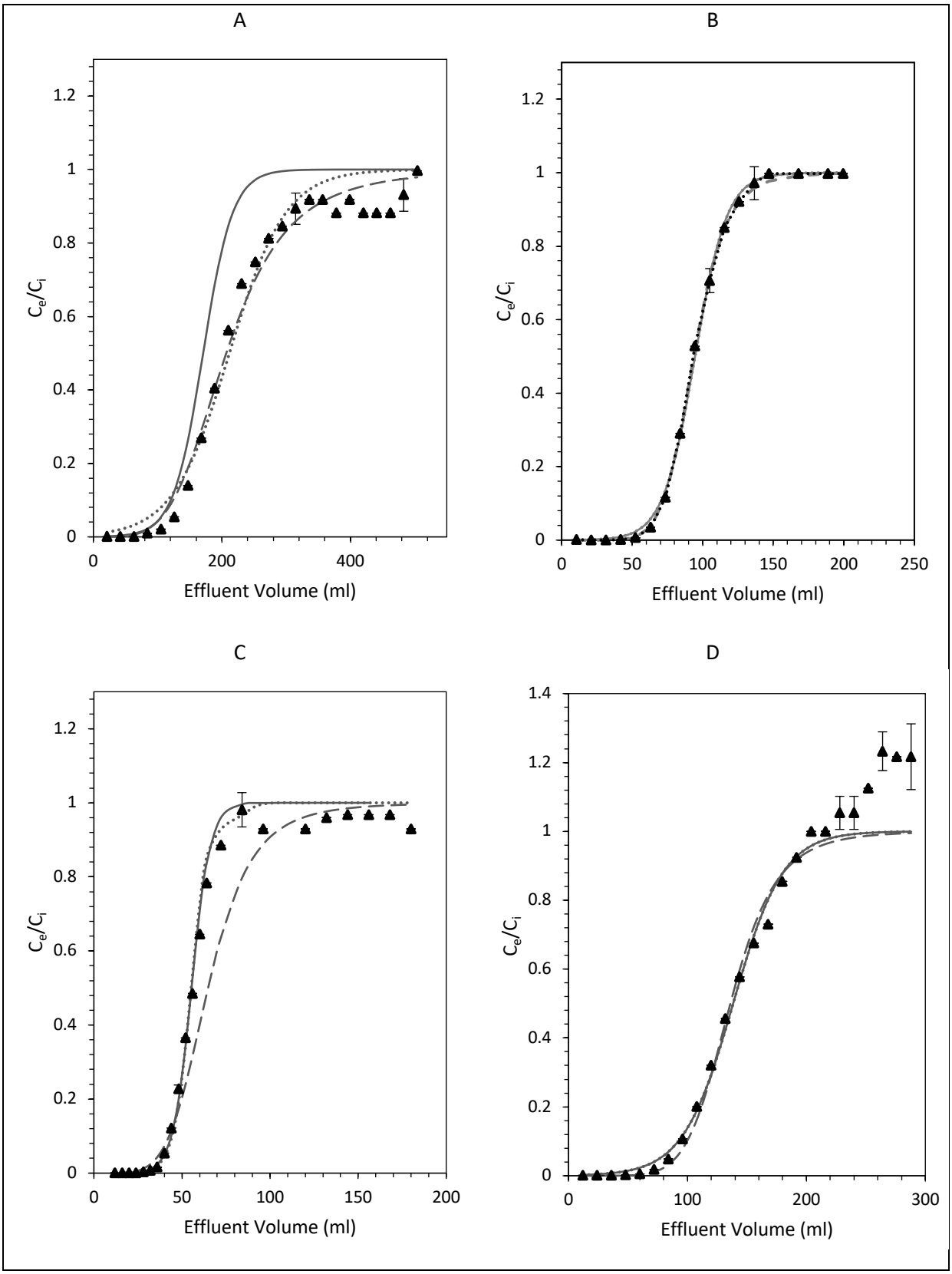

Figure 5. Column behaviour of Purolite MTS9850 with a variety of solutions; A = 5 g L^{-1} iodide only, B = 5 g L^{-1} iodide and 5 g L^{-1} nitrate, C = 5 g L^{-1} iodide and 5 g L^{-1} molybdate, D = 5 g L^{-1} iodide and 5 g L^{-1} iodine. Resin BV = 4 mL. Flow rate = 5.25 BV hr^{-1}. T = 20°C. Breakthrough models used indicated by lines on the plots; solid grey line = Thomas, grey dotted line = Yoon Nelson, grey dashed line = Dose Response.

The breakthrough data were fitted to the four models previously described. Results of the Adams-Bohart model-fitting are not presented, due to poor agreement. The Thomas, Yoon-Nelson and Dose-Response models for each co-contaminant are provided for comparison to experimental data.

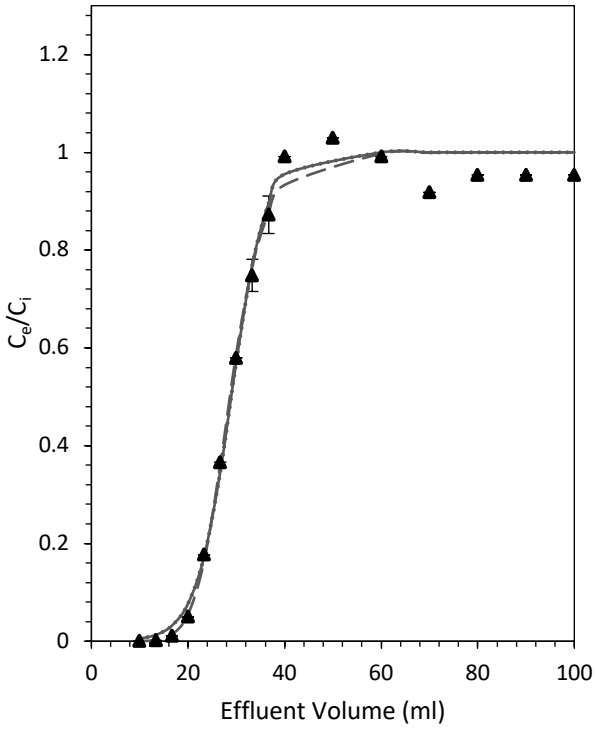

Figure 6. Column behaviour of Purolite MTS9850 with iodide and all co-contaminants 5 g L^{-1} iodide, nitrate, molybdate and iodine. Resin BV = 4 mL. Flow rate = 5.25 BV hr^{-1}. T = 20°C. Breakthrough models used to fit are indicated by lines on the plots; solid grey line = Thomas, grey dotted line = Yoon Nelson, grey dashed line = Dose Response.

3.4. Resin characterization

3.4.1. Elemental Analysis

Elemental analysis was carried out to determine the nitrogen content of the two resins and investigate whether this could be correlated to uptake capacity. Results are shown in Table 4.

Table 4. Measured carbon, hydrogen, nitrogen and chlorine content for two resins.

Resin	Carbon %	Hydrogen %	Nitrogen %	Chlorine %
Purolite MTS9850	38.7 ± 0.2	7.78 ± 0.05	14.7 ± 0.1	23.1 ± 0.3
Lewatit A365	38.2 ± 0.2	7.42 ± 0.05	15.8 ± 0.1	22.2 ± 0.4

3.4.2. FT-IR Spectroscopy

Spectra were produced for samples of resin that had been pre-conditioned in 1 M HNO_3 for 24 hours, as well as samples that had been contacted with a solution of 5 g L^{-1} iodide and 5 g L^{-1} iodine. Figure 7 presents comparisons of the two resins for pre-iodide contact and post-contact with the iodide-iodine solution for the region of 3500 – 2500 cm^{-1}, showing differences in the C-H stretch region. Full spectra for each individual resin are available in the Supporting Information, Fig. S.1 and S.2, while peak identification tables are available in Tables S.1 and S.2.

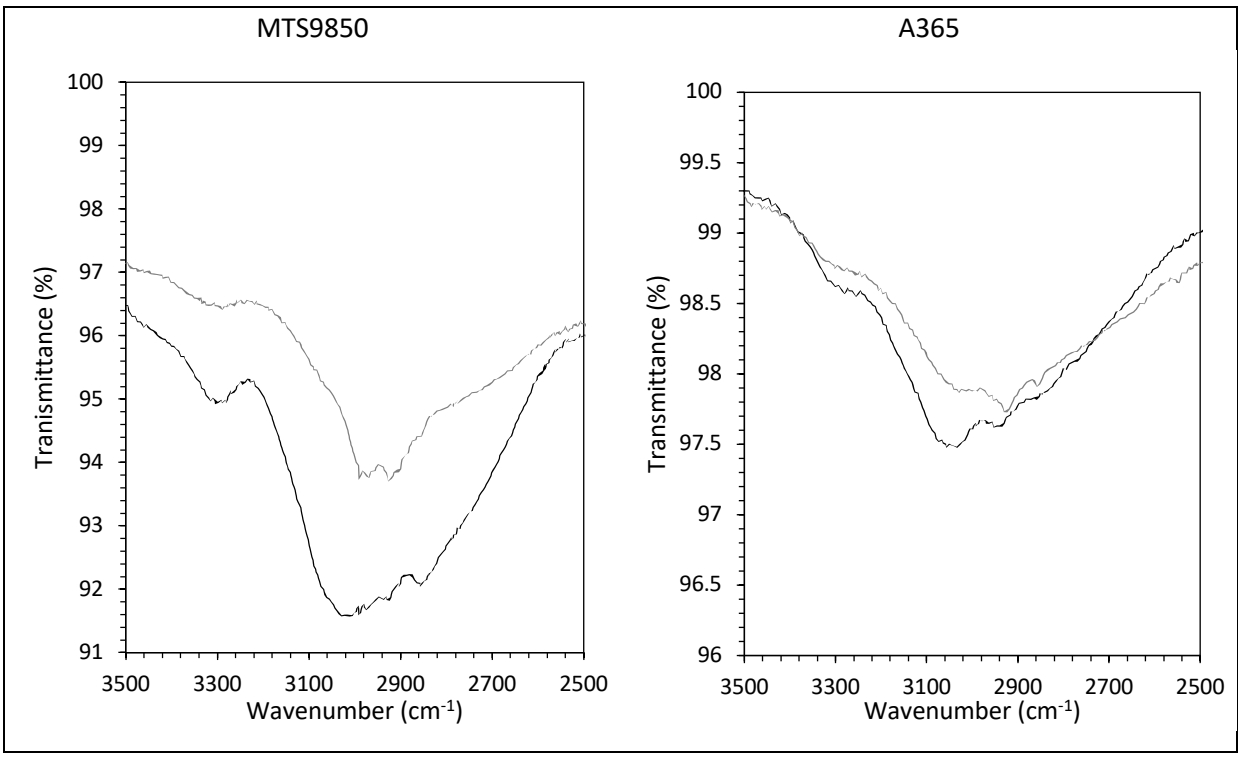

Figure 7. FT-IR spectra for the region of 3500-2500 cm^{-1} for WBA resins pre- and post-contact with iodide/iodine solutions. Black line = pre-contact. Grey line = post-contact.

3.4.3. Raman Spectroscopy

Raman spectroscopy was performed to determine the presence of the triiodide ions on the resin surface for samples contacted by the iodide/iodine system. Both resins returned near-identical spectra (Figure 8), with peak assignments possible in the region of 50-300 cm^{-1}, which are presented in Table 5. At higher wavenumbers, the spectra could not be interpreted, due to saturation, produced by the fluorescent properties of the samples.

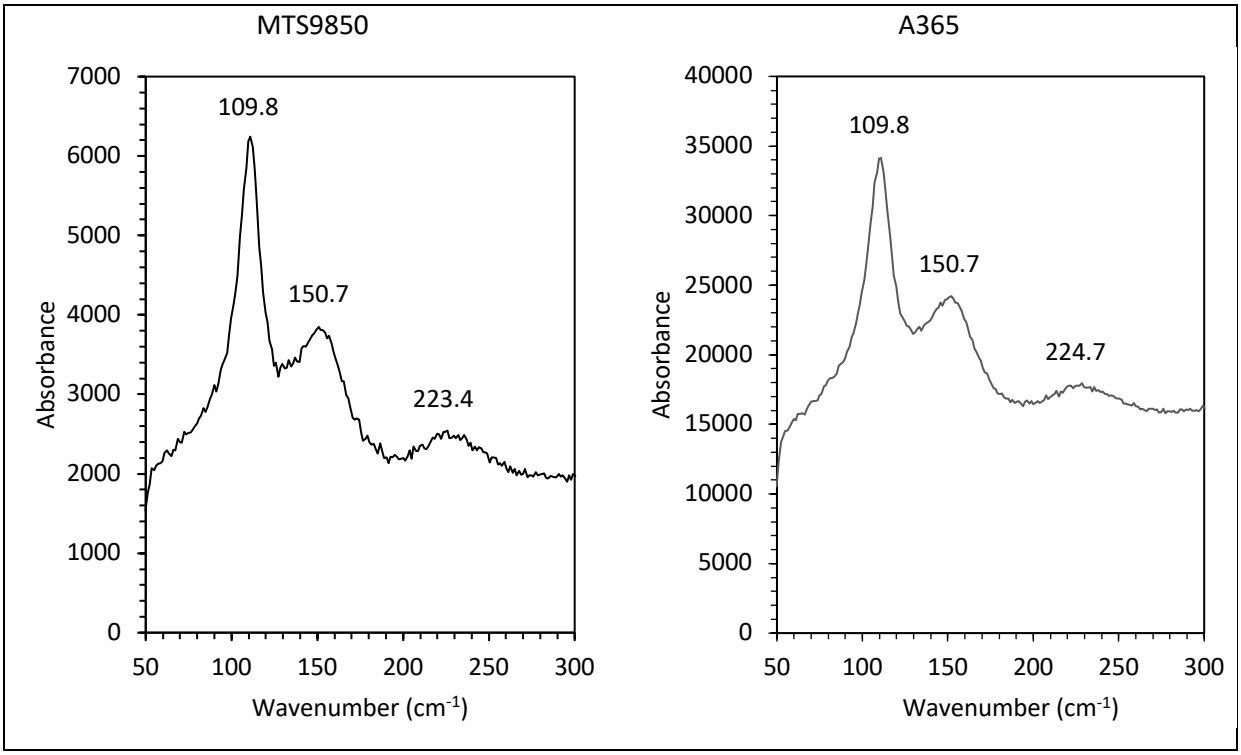

Figure 8. Raman spectra for the WBA resins post-contact with iodide/iodine solution. Spectra show the region in which iodine species produce notable peaks.

Table 5. Assignments of Raman spectral peaks for the two resins.

Wavenumber (cm^{-1})	**Assignment**
223.4 (MTS9850)/ 224.7 (A365)	I_3^- $2v_1$ symmetric stretch
150.7	I_3^- v_1 asymmetric stretch
109.8	I_3^- v_1 symmetric stretch

4. Discussion

4.1. pH effects on iodide extraction

The iodide uptake of both resins was high across the majority of the pH range tested. Above pH 6 the extraction of iodide starts to be suppressed, with the lowest extraction values achieved at pH 10 for both resins. It is seen that Purolite MTS9850 demonstrates higher uptake capacities across all pHs, apart from pH 10. Results therefore suggest that Lewatit A365 is potentially more effective in more alkaline conditions, while MTS9850 is superior in acidic conditions, which is the focus of this work. Alkaline and neutral conditions have been included here, as iodide removal could potentially be desirable from other waste-streams, such as medical waste [29]. The greater dependency of pH on MTS9850 iodide uptake could be partly attributed to the aromatic alcohol present in the MTS9850 functionality, which would be protonated and act as an anion-exchange site at very low pH. From the data captured at pH 9-10, it can be inferred that the average pk_a of protonated ammonium sites on the resins is higher for A365. This is concurrent with the functional group structures, with A365 consisting of 1° amines and MTS9850 containing 2° and 3° amines [30, 31].

There is no obvious optimum pH observed for either resin, with very little change in iodide uptake under acidic conditions. It is known from the literature that high ionic strength suppresses the anion exchange mechanism, and from this it can be predicted that the extraction of iodide under concentrated acid conditions would be suppressed [17], as well as the resin potentially degrading. The uptake capacities for iodide were lower than would be expected, given the subsequent isotherm data. This can be explained by the HNO_3 used for pH adjustments suppressing iodide uptake, due to the competition between iodide and introduced nitrate ions. This competition would be present in the aqueous system, which the proposed treatment would target, since the UNF waste-stream is dissolved in concentrated nitric acid and is an industrial consideration.

4.2. Co-contaminant effect on iodide extraction

It can be observed from Figure 3 that MTS9850 has superior uptake, compared to A365, in the presence of competing anions. It is clear that molybdate has a stronger suppressive effect as can be

seen by the steeper gradients corresponding to addition of molybdate. It can be concluded that the selectivity of the two resins for the different anions are as follows:

$$MoO_4^{2-} > NO_3^- > I^-$$

It is generally difficult to obtain iodide selectivity data against competing anions, as relevant literature on WBA resin behaviour is lacking. Resins will often have specific selectivity for anions, dependent on factors such as crosslinking and specific functionality. Concentration and experimental conditions have also been seen to alter the selectivity. However, Gierczyk *et al.* studied gel-like polymers with WBA functionality and the same selectivity series to that suggested in this work was determined [32].

Interestingly, the introduction of iodine to the system appeared to increase the uptake of iodide from the solution. Iodine speciation is not only dependent upon pH, temperature and redox potential of the solution, but also on the equilibrium formed between iodide, iodine and triiodide (Eq. (12)).

$$I_2 + I^- \leftrightharpoons I_3^- \quad (12)$$

Triiodide can also be formed through the reduction of iodine (Eq. (13)), which can then undergo a further redox reaction, ultimately leading to the reformation of iodide (Eq. (14)) and potentially increasing the uptake via changing the concentration gradient [33, 34].

$$3I_2 + 2e^- \leftrightharpoons 2I_3^- \quad (13)$$

$$I_3^- + 2e^- \leftrightharpoons 3I^- \quad (14)$$

Wiebenga *et al.* identified that aqueous triiodide concentration increases with the acidity of the system and therefore iodide could feasibly be reformed, as previously mentioned [35]. The equilibrium constant for Eq. (12) however, is 4.76×10^{-3} [36], which suggests iodide uptake should not increase significantly, as is observed in this work. However, this obviously does not consider the effects of the interface between the hydrophobic resin and the aqueous environment. Our proposed reasoning for this behaviour, based on solid-state analysis, will be discussed in section 4.5.

The near linear correlation observed between iodide uptake and co-contaminant concentration, for all three species tested could be used to potentially predict the effect on resin performance industrially.

4.3. Isotherm behaviour for anion extraction

For both resins, the D-R isotherm model provided excellent description of the uptake. Hence it can be inferred that both A365 and MTS9850 possess an approximately Gaussian distribution of binding site energies [37]. The experimental E_D values of 8.60 (MTS9850) and 8.76 (A365) are consistent with the expected uptake mechanism. Values below 8 kJ mol^{-1} relate to a physical adsorption process, values between 8 and 16 kJ mol^{-1} correspond to an ion-exchange process and values exceeding 16 kJ mol^{-1} infer a stronger chemical adsorption process [38].

Data was fitted to the Freundlich isotherm model to investigate potential multilayer adsorption behaviour. This model gives a superior fit for MTS9850 uptake and this suggests a weaker physisorption interaction may become prevalent at higher C_i, which may also contribute to the greater capacity of this resin. For both resins, the heterogeneity factor, n, exceeds a value of 1. Values greater than 1 indicate an element of heterogeneity of the binding sites on the resin's surface [39]. The returned values between 2.5 – 3 suggest the binding sites in this instance are relatively heterogeneous [40].

With respect to the Temkin isotherm model, the positive B values for both resins, albeit less than 1 kJ mol^{-1}, suggest a weak physisorption process is prevalent. Values for b_T are also positive, confirming that the adsorption process is exothermic. This model fitted the data moderately well and suggested a linear trend between heat of adsorption and surface coverage for these systems [41].

In comparison to previous studies on anion-exchange using WBA resins, the iodide capacity of these resins exceeds that of other sorbents previously reported. The maximum loading values, calculated by both Langmuir and D-R isotherm fitting are actually in excess of the manufacturer-quoted

capacities, considerably so in the case of MTS9850 (Table 1). It is known that WBA resins tend to favourably exchange larger ions, as well as those with a greater charge, due to strong electrostatic interactions. The superior capacity of MTS9850 was unexpected, given that its manufacturer-quoted exchange capacity is lower (Table 1). This table however, also shows the greater moisture content of MTS9850 when hydrated. It is known that this parameter corresponds to a higher porosity and a greater selectivity for larger ions such as iodide. Furthermore, the macroporous nature of MTS9850 allows for greater access to the interior exchange sites and is also directly linked to an increased level of crosslinking, which in turn increases moisture content. It is probable that MTS9850 has a greater percentage of crosslinking with the divinylbenzene backbone resulting in its greater moisture content. MTS9850 also has a smaller average bead size, meaning a shorter diffusion pathway to the active sites in the macroporous structure and subsequently an increased likelihood of interaction with the protonated functional groups [16].

There are few direct literature comparisons to be made with respect to iodide uptake. However, Table 6 shows uptake capacities of a number of anion-exchange resins for a range of other anions, showing that the two resins used in this study are superior in capacity to any WBAs that have been documented. A study featuring uranyl uptake by Purolite MTS9850 has been included, which confirms the excellent capacity of this resin.

Table 6. A comparison of uptake capacities for various ions and WBAs to provide a comparison to the two resins used in this study.

Resin	Matrix	Functionality	Target Ion	Uptake capacity (q_{max})	Ref
Duolite A368	PS-DVB	2° amine	Iodide ($^{131}I^-$)	62.25 mg g^{-1}	[42]
			Bromide (^{82}Br)	34.52 mg g^{-1}	[42]
Duolite A7	PFA-PC	2° amine	Nitrate (NO_3^-)	6.51 mg g^{-1}	[43]
Amberlyst A21	PS-DVB	2° amine	Sulphate (SO_4^{2-})	16.18 mg ml^{-1}	[44]
Amberlite IRA-67	PA-DVB	3° amine	Phosphate (PO_4^{3-})	120.63 mg g^{-1}	[45]
Purolite MTS9850	PA-DVB	Polyamine	Uranyl ($[UO_2(SO_4)_3]^{4-}$)	269.50 mg g^{-1}	[46]

PS-DVB = polystyrene divinylbenzene, PFA-PC = crosslinked phenol-formaldehyde polycondensate, PA-DVB = polyacrylic divinylbenzene.

It is clear that the two resins studied are suitable for anion uptake, as their capacities are unusually high, far exceeding many other commercially available materials. A key point appears to be that the resins identified for comparison with polystyrene-DVB backbones have considerably lower exchange capacities. The Amberlite IRA-67, used by Drissi and Mouats [45], as well as the resins used in this work, have polyacrylic-DVB backbones and exhibit higher uptake capacity values. Other iodide uptake studies tend to look at strong base resins, which display considerably different uptake behaviours [8, 47, 48].

The quoted ion-exchange capacity of the two resins, in mmol g^{-1}, was calculated from manufacturer specifications given in Table 1 and using the experimentally-determined ratio between wet settled volume and dry mass. For A365, this was found to be 6.8 mmol g^{-1}, compared to our experimental value, derived from the D-R isotherm, of 4.64 mmol g^{-1}. For MTS9850, the specification was 5.5 mmol g^{-1}, compared to the experimental value of 5.99 mmol g^{-1}. From these calculations, it can be seen that MTS9850 performed slightly above expectations, based on manufacturer data. This may indicate an interaction between resin-bound and aqueous iodide occurs at very high C_i, allowing for further adsorption and hence the good fitting to the Freundlich model. The poorer performance of A365, relative to manufacturer data may be partially explained by the presence of amide nitrogens in the functionality of A365 (Figure 1). These would be expected to be very weakly basic and not significant exchange sites at the natural pH of the sodium iodide solutions. Notably, for MTS9850, the capacity is seen to be significantly greater than for uranyl uptake observed by Amphlett *et al.* [46]. This however, was a chelating interaction, with a single uranyl anion interacting with multiple amines.

Other materials have focussed on removal of radioiodine from the gaseous phase and uptake values are less comparable. Some studies have investigated adsorption of pure iodine vapour, rather than iodide/iodine in solution and with competing anions. Chalcogels with NiMoS and ZnSnS matrices achieved uptakes of 2.25 g I_2 g^{-1} [49] and a hydrogen-bonded, cross-linked organic framework

achieved an uptake of 2.9 g I_2 g^{-1} at 75 °C [50]. Such sorbents have high iodine-capture potential, but their synthesis has not yet transitioned to an industrially viable scale.

4.4. Fixed-bed column dynamics for anion extraction

For the solution of iodide only, the Dose-Response model provided an excellent fit for experimental data, closely followed by the Yoon-Nelson model. The Thomas model did not adequately describe the data in comparison. It is observed that with the introduction of nitrate and molybdate ions, breakthrough time is much shorter as would be expected, due to the selectivity of these competing ions, as previously mentioned. It can also be seen that the iodide/nitrate system breakthrough curve has a shallower gradient than the iodide/molybdate system (Fig 5B and 5C). This suggests iodide ions were competing more strongly for the binding sites, which is in agreement with the batch co-contaminant data.

For the iodide/iodine system, the dynamic models demonstrate good fits until breakthrough is achieved, as at this point the concentration of iodide continued increasing beyond the inlet solution concentration (Fig. 5D). We believe that the initial solution was in a state of equilibrium with the iodide, iodine and triiodide ion, but as the experiment progressed, triiodide bound to the active sites and/or the surface of the resin (see Section 4.5.) and may have ultimately been remobilised back into the aqueous phase with the subsequent flow and dissociated into iodide and iodine, hence the eluent having a higher iodide concentration that the inlet solution.

For the iodide/iodine system, the 50% breakthrough time was greater than for all other co-contaminants (692 minutes) as calculated by Yoon-Nelson model, but less than the iodide only system, while a similar uptake capacity to nitrate and molybdate experiments was observed. This suggests that in column operation, at least under these experimental conditions, the addition of iodine may not enhance iodide uptake to the extent that column operating lifespan would also be lengthened. Hence, the proposed triiodide formation on the resin seems to be a relatively slow kinetic process. The effect of all co-contaminants added at the same time produced the shortest breakthrough time observed in this study, (174 minutes), as there were two competing anions at

high concentrations in the inlet solution. Overall, despite the obvious effects of co-contaminants, the dynamic capacity of S985 for iodide is still considerable and the close fitting to theoretical models means that column breakthrough behaviour would be easy to predict with all species present, which would be an advantage industrially.

A number of studies have considered iodine uptake in a dynamic environment. However, the lack of dynamic modelling means there are no comparable parameters [8, 48, 51]. There are no previous studies, to the best of our knowledge on dynamic experiments, using WBAs for iodide uptake. However, some novel adsorbents have been so tested and results are summarised in Table 7. This table includes results for some commercial ion-exchange resins with different targeted anions. It can therefore be seen that MTS9850 has a rather greater iodide capacity than other adsorbents, in dynamic, as well as static conditions. A relevant comparison is the work of Li and Yang [55], who used Hydrolite 202, with nitrite as the target anion, since the suppression by nitrate on uptake was considered. It was found that nitrate suppressed nitrite uptake by ~42% when compared to the initial experiment, which is comparable to this work.

Table 7. A comparison of various ion exchange material uptakes in a dynamic environment to demonstrate Purolite MTS9850 (used in this study) is superior to other dynamic studies in literature.

Sorbent name	Matrix	Functionality	Target ion	Capacity (q_{max})	Ref
Mg-Al double hydroxides	Porous silica spheres	-	Iodide ($^{127}I^-$)	81.28 mg g^{-1}	[52]
Modfied poly(glycidyl methacrylate) (MPGMA)	Poly(glycidyl methacrylate)	Hydroxylamine	Iodide ($^{131}I^-$)	~ 25 mg g^{-1}	[53]
Amberlyst A21	PS-DVB	2° amine	Sulphate (SO_4^{2-})	12.7 mg ml^{-1}	[44]
Purolite A520E	PS-DVB	4° ammonium	Nitrate (NO_3^-)	9.69 mg g^{-1}	[54]
Hydrolite 202	PS-DVB	4° ammonium	Nitrite (NO_2^-)	46.80 mg g^{-1}	[55]

4.5. Resin Characterization

4.5.1. Elemental Analysis

Static isotherm work showed that the capacity of MTS9850 for iodide ions was considerably greater. It was therefore hypothesised that it would exhibit a greater nitrogen mass %, corresponding to a greater number of amine groups and hence a better degree of functionalization.

A365 was actually found to contain a slightly higher nitrogen mass % than MTS9850. However, given the apparent maximum iodide uptakes seen in Table 2, this cannot be directly correlated to the number of accessible anion-exchange sites, for which MTS9850 is superior. This may again be explained, by the presence of unprotonated amide nitrogens in the A365 functionality, whereas the majority of nitrogen atoms in the MTS9850 functionality are 2° amines. The nitrogen content of the resin functional group, after mass correction to account for the different counterions in uptake experiments, was 8.59 and 9.68 mmol g^{-1} for MTS9850 and A365 respectively, from which it appears that, despite the high iodide uptake capacities observed, not every nitrogen represents an active exchange site for either resin, since the maximum iodide uptake in mmol g^{-1} does not approach these levels (6.0 and 4.6 mmol g^{-1} respectively). Another possibility is that, due to the vicinity of heteroatoms within the functional group of MTS9850, some of the large iodide ions interact with multiple nitrogens upon binding, which would also help explain the observed heterogeneity of the adsorption, derived from Freundlich isotherm fitting. This may indeed be true for most common anions, which would explain why the manufacturer-specified exchange capacity for MTS9850 (Table 1) is lesser.

It is also noted from the elemental analysis that the measured chlorine mass % for MTS9850, which was assumed to be entirely chloride counterions from the HCl pretreatment, equated to a capacity of 6.51 mmol g^{-1}, which was close to, but slightly above the theoretical maximum uptake capacity observed for iodide (Table 2).

4.5.2. FT-IR Spectroscopy

FT-IR spectra show that the C-H stretch region in both resins undergoes notable shifts when iodine is introduced into the system. Specifically, the ratio of intensity between aromatic and aliphatic C-H peaks appears to alter. We believe this represents the formation of a charge transfer (CT) complex, with triiodide acting as the electron-acceptor. Previous studies have demonstrated that iodine, in various forms, can act as a σ-acceptor with aliphatic molecules and aromatic systems [56, 57]. Refat *et al*. investigated CT complex-formation between morpholine and triiodide and also observed significant changes in the N-H stretch region [56]. Mahmoud *et al*. postulated a CT interaction between triiodide and the primary amine groups of amino acids [58]. However, this is difficult to correlate in our work because of the broadness and weakness of the N-H stretch peak, caused by the polymeric environment. Nonetheless, the decrease in aromatic C-H stretch peak intensity, first observed by Benesi and Hildebrand, is obvious (Figure 7) and is believed to be the result of protons detaching from the aromatic ring and forming hydrogen iodide [59]. The likelihood of complexation increases when a greater number of π-electrons are present in a localised area, such as in an aromatic structure. However, if the electron density spreads over a larger area (i.e. multiple rings), the stability of the complex is hindered [60, 61]. Neither resin matrix features an extended delocalised π-system as the aromatic rings are instead crosslinked by aliphatic hydrocarbons. Hence CT complex formation would be predicted to be favourable. To the best of our knowledge, this is the first time such interaction has been reported between iodine and a polymeric resin.

4.5.3. Raman Spectroscopy

Raman spectroscopy produced three notable peaks present at 111 cm^{-1}, 153 cm^{-1} and 225 cm^{-1}, which can all be attributed to the presence of triiodide on the resin surfaces [62, 63].

The absence of a stronger peak at ~160 -170cm^{-1} indicates there is not significant polyiodide or diiodine formation on the resin [64]. It has been observed in the literature that CT complexes existing in hydrophobic conditions lead to triiodide being the dominant species [58], whereas crystalline and ionic liquid environments produce polyiodides [64, 65]. Indeed, it is known that the

equilibrium constant of Eq. (12) in a more hydrophobic environment is pushed in favour of triiodide formation [66]. Hence, the observations in this study are predictable.

The likely uptake mechanism involves molecular iodine associating with the hydrophobic areas of the resin, consistent with the CT complex formation suggested by the IR and Raman spectra, followed by a surface reaction with aqueous iodide. This phenomenon explains the enhanced uptake of iodide observed with the iodide/iodine systems in batch experiments, as more adsorption sites are theoretically created.

5. Conclusions

Two commercial weak base anion exchange resins, Purolite MTS9850 and Lewatit A365 were assessed for their suitability in the removal of radioiodine from spent nuclear fuel reprocessing aqueous waste streams. The resins achieved maximum uptakes of 761 ± 14 mg g^{-1} and 589 ± 15 mg g^{-1} respectively from Dubinin-Radushkevich isotherm modelling. These values exceeded those reported for currently implemented industrial adsorbents such as silver-impregnated zeolites and silicas.

MTS9850 exhibited lower nitrogen mass % than A365, yet appeared to exhibit more active exchange sites. Its superior uptake capacity may be attributed to other physical characteristics such as moisture content and a higher percentage of crosslinking within the polymer backbone.

For both resins, iodide uptake increased with decreasing pH, which would be advantageous in the acidic conditions present in UNF raffinate. The introduction of co-contaminants nitrate and molybdate reduced iodide uptake, as would be expected for the weak base anion functionality. However, iodide uptake increased with the addition of diiodine to the system. The proposed CT complex formation and triiodide formation observed have not previously been documented for polymeric resins and such phenomena could potentially be exploited for improved resin performance industrially.

Equilibrium uptake data were fitted to isotherm models. Both resins showed good agreement with the D-R model, with A365 also following the Langmuir model closely, suggesting monolayer adsorption, while MTS9850 followed the Freundlich model accurately, suggesting multilayer adsorption was occurring. The nature of the polyamine functionality, with many slightly different tertiary amine groups present, is likely the cause of the heterogeneity of binding sites observed. Dynamic studies on MTS9850 concluded the research and column behaviour followed the Dose-Response and Yoon-Nelson models accurately.

It is hoped that this work will provide a foundation for the use of polyamine functionality in the capture of radioiodine from aqueous waste-streams of the nuclear industry, for which there is currently a lack of definitive, economical solutions.

Conflicts of interest

The authors declare no conflicts of interest.

Acknowledgements

The authors would like to thank Stephen Atkin of the Department of Chemistry at The University of Sheffield for providing elemental analysis of the resins and Purolite and Lanxess for the resin donations. We would also like to thank members of the Separations and Nuclear Chemical Engineering Research (SNUCER) group, who have all provided support and help, both in and outside of the laboratory. This work was supported by the Engineering and Physical Sciences Research Council through the UK Korea Civil Nuclear Energy program grant EP/M026558/1 Silicate Nanoparticles for Extraction of Radionuclides (SINNER).

References

[1] A. Koning, R. Forrest, M. Kellett, R. Mills, H. Henriksson, and Y. Rugama, “The JEFF-3.1 Nuclear Data Library,” JEFF Report 21, 2006.

[2] N. R. Soelberg et al., “Radioactive Iodine and Krypton Control for Nuclear Fuel Reprocessing Facilities,” Sci. Technol. Nucl. Install., 1–12, 2013.

[3] E. F. da Silva, “Geochemistry and Environmental Mobility of Iodine-129,” in International Nuclear Atlantic Conference - INAC 2005, 2005.

[4] National Academy of Sciences, Exposure of the American People to Iodine-131 from Nevada Nuclear-Bomb Tests: Review of the National Cancer Institute Report and Public Health Implications. 1999.

[5] Agency for Toxic Substances and Disease Registry, “Radiation Exposure from Iodine 131,” 2002.

[6] P. N. Swift and W. M. Nutt, “Applying Insights from Repository Safety Assessments to Evaluating Impacts of Partitioning and Transmutation,” in Actinide and Fission Product Partitioning and Transmutation, 2010, pp. 1–22.

[7] S. Fukuda et al., “Global searches for microalgae and aquatic plants that can eliminate radioactive cesium, iodine and strontium from the radio-polluted aquatic environment: a bioremediation strategy,” J. Plant Res., 127, 79–89, 2014.

[8] P. K. Sinha, K. B. Lal, and J. Ahmed, “Removal of radioiodine from liquid effluents,” Waste Manag., 17, 33–37, 1997.

[9] Y. V. Zabaluev, “Management of radionuclides from reprocessing plant gaseous effluents,” IAEA Bulletin 21,”1979.

[10] B. J. Riley, J. D. Vienna, D. M. Strachan, J. S. McCloy, and J. L. Jerden, “Materials and processes for the effective capture and immobilization of radioiodine: A review,” J. Nucl. Mater., 470, 307–326, 2016.

[11] R. Fuge and C. C. Johnson, “Iodine and human health, the role of environmental geochemistry and diet, a review,” Appl. Geochemistry, 63, 282–302, 2015.

[12] IAEA, Ion Exchange Technology in the Nuclear Fuel Cycle. 1986.

[13] J. G. Moore and W. B. Howerton, “LMFBR Fuel Cycle Studies Progress Report for December 1970,” 1971.

[14] D. W. Holladay, “A literature survey: methods for the removal of iodine species from off-gases and liquid waste streams of nuclear power and nuclear fuel reprocessing plants, with emphasis on solid sorbents,” 1979.

[15] K. E. Parker, E. C. Golovich, and D. M. Wellman, “Iodine Adsorption on Ion-Exchange Resins and Activated Carbons - Batch Testing,” 2014.

[16] F. J. DeSilva, “Essentials of Ion Exchange,” in 25th Annual WQA Conference, 1999.

[17] O. N. Kononova, A. M. Melnikov, and D. S. Demitrichenko, “Simultaneous Ion Exchange Recovery and Subsequent Separation of Platinum(II, IV), Rhodium(III), and Nickel(II) from Chloride and Sulfate-Chloride Solutions,” Solvent Extr. Ion Exch., 31, 306–319, 2013.

[18] A. N. Nikoloski, K.-L. Ang, and D. Li, “Recovery of platinum, palladium and rhodium from acidic chloride leach solution using ion exchange resins,” Hydrometallurgy, 152, 20–32, 2015.

[19] A. A. Susoyeva, A. A. Blokhin, Y. V. Murashkin, and M. A. Mikhaylenko, “Sorption recovery of rhodium(III) from multicomponent chloride solutions in the presence of tin(II) chloride,” Russ. J. Non-Ferrous Met., 57, 681–685, 2016.

[20] N. Reynier, R. Lastra, C. Laviolette, J.-F. Fiset, N. Bouzoubaâ, and M. Chapman, “Comparison of Uranium Recovery by Ion Exchange from Sulfuric Acid Liquor in Iodide and Chloride Media,” Solvent Extr. Ion Exch., 34, 188–200, 2016.

[21] N. Ayawei, A. N. Ebelegi, and D. Wankasi, “Modelling and Interpretation of Adsorption Isotherms,” J. Chem., 1–11, 2017.

[22] Y. S. Ho, J. F. Porter, and G. McKay, “Equilibrium Isotherm Studies for the Sorption of Divalent Metals Ions onto Peat: Copper, Nickel and Lead Single Component Systems,” Water, Air Soil Pollut., 141, 1–33, 2002.

[23] H. N. Tran, S.-J. You, and H.-P. Chao, “Effect of pyrolysis temperatures and times on the adsorption of cadmium onto orange peel derived biochar,” Waste Manag. Res., 34, 129–138, 2016.

[24] Y. S. Ho, “Isotherms for the Sorption of Lead onto Peat: Comparison of Linear and Non-Linear Methods,” Polish J. Environ. Stud., 15, 81–86, 2006.

[25] M. Belhachemi and F. Addoun, “Comparative adsorption isotherms and modeling of methylene blue onto activated carbons,” Appl. Water Sci., 1, 111–117, 2011.

[26] K. Vijayaraghavan, T. Padmesh, K. Palanivelu, and M. Velan, “Biosorption of nickel(II) ions onto Sargassum wightii: Application of two-parameter and three-parameter isotherm models,” J. Hazard. Mater., 133, 304–308, 2006.

[27] A. A. Inyinbor, F. A. Adekola, and G. A. Olatunji, “Kinetics, isotherms and thermodynamic modeling of liquid phase adsorption of Rhodamine B dye onto Raphia hookerie fruit epicarp,” Water Resour. Ind., 15, 14–27, 2016.

[28] R. Hema Krishna and A. V. V. S. Swamy, “Physico-Chemical Key Parameters, Langmuir and Freundlich isotherm and Lagergren Rate Constant Studies on the removal of divalent nickel from the aqueous solutions onto powder of calcined brick,” Int. J. Eng. Res. Dev., 4, 29–38, 2012.

[29] R. Ravichandran, J. Binukumar, and A. Al Saadi, “Estimation of effective half life of clearance of radioactive Iodine (131 I) in patients treated for hyperthyroidism and carcinoma thyroid,” Indian J. Nucl. Med., 25, 49, 2010.

[30] A. V. Rayer, K. Z. Sumon, L. Jaffari, and A. Henni, “Dissociation Constants (pKa) of Tertiary and Cyclic Amines: Structural and Temperature Dependences,” J. Chem. Eng. Data, 59, 3805–3813, 2014.

[31] J. A. Dean, Lange’s Handbook of Chemistry 15th Edition. 1998.

[32] B. Gierczyk, M. Cegłowski, and M. Zalas, “New Gel-Like Polymers as Selective Weak-Base Anion Exchangers,” PLoS One, 10, 2015.

[33] G. Boschloo and A. Hagfeldt, “Characteristics of the Iodide/Triiodide Redox Mediator in Dye-Sensitized Solar Cells,” Acc. Chem. Res., 42, 1819–1826, 2009.

[34] C. L. Bentley, A. M. Bond, A. F. Hollenkamp, P. J. Mahon, and J. Zhang, “Voltammetric Determination of the Iodide/Iodine Formal Potential and Triiodide Stability Constant in Conventional and Ionic Liquid Media,” J. Phys. Chem. C, 119,. 22392–22403, 2015.

[35] E. H. Wiebenga, E. E. Havinga, and K. H. Boswijk, “Structures of Interhalogen Compounds and Polyhalides,” in Advances in Inorganic Chemistry and Radiochemistry, 1961, pp. 133–169.

[36] O. N. Starovoytov, N. S. Kim, and K. N. Han, “Dissolution behaviour of silver in ammoniacal solutions using bromine, iodine and hydrogen-peroxide as oxidants,” Hydrometallurgy, vol. 86, 114–119, 2007.

[37] S. E. Pepper, K. R. Whittle, L. M. Harwood, J. Cowell, T. S. Lee, and M. D. Ogden, “Cobalt and nickel uptake by silica-based extractants,” Sep. Sci. Technol., 53, 1552–1562, 2018.

[38] F. G. Helfferich, Ion Exchange. 1962.

[39] I. A. W. Tan, A. L. Ahmad, and B. H. Hameed, “Adsorption isotherms, kinetics, thermodynamics and desorption studies of 2,4,6-trichlorophenol on oil palm empty fruit bunch-based activated carbon,” J. Hazard. Mater., 164, 473–482, 2009.

[40] R. J. Umpleby, S. C. Baxter, A. M. Rampey, G. T. Rushton, Y. Chen, and K. D. Shimizu, “Characterization of the heterogeneous binding site affinity distributions in molecularly imprinted polymers,” J. Chromatogr. B, 804, 141–149, 2004.

[41] M. R. Samarghandi, M. Hadi, S. Moayedi, and F. Barjasteh Askari, “Two-Parameter Isotherms of Methyl Orange Sorption by Pinecone Derived Activated Carbon,” Iran. J. Environ. Heal. Sci. Eng., 6, 285–294, 2009.

[42] P. U. Singare, “Performance Based Evaluation of Industrial Grade Resins Duolite ARA-9366 and Duolite A-368,” Kem. u Ind., 63, 245–252, 2014.

[43] M. Nujić, D. Milinković, and M. Habuda-Stanić, “Nitrate removal from water by ion exchange,” Croat. J. Food Sci. Technol., 9, 182–186, 2017.

[44] D. Guimarães and V. A. Leão, “Batch and fixed-bed assessment of sulphate removal by the weak base ion exchange resin Amberlyst A21,” J. Hazard. Mater., 280, 209–215, 2014.

[45] R. Drissi and C. Mouats, “Removal of Phosphate by Ion Exchange Resin: Kinetic and Thermodynamic Study,” Rasayan J. Chem., 11, 1126–1132, 2018.

[46] J. T. M. Amphlett, M. D. Ogden, R. I. Foster, N. Syna, K. Soldenhoff, and C. A. Sharrad, “Polyamine functionalised ion exchange resins: Synthesis, characterisation and uranyl uptake,” Chem. Eng. J., 334, 1361–1370, 2018.

[47] P. U. Singare, “Ion-Isotopic Exchange Reaction Kinetics in Characterization of Anion Exchange Resins Dowex 550A LC and Indion-820,” Open-Access J. Basic Princ. Diffus. Theory, Exp. Appl., 19, 1–21, 2013.

[48] C.-C. Lin and J. J. Younger, “Adsorption of Iodine Species with Ion Exchange Resins in Aqueous Solutions,” Nucl. Technol., 47, 468–476, 1980.

[49] K. S. Subrahmanyam et al., “Chalcogenide Aerogels as Sorbents for Radioactive Iodine,” Chem. Mater., 27, 2619–2626, 2015.

[50] Y. Lin et al., “An Elastic Hydrogen-Bonded Cross-Linked Organic Framework for Effective Iodine Capture in Water,” J. Am. Chem. Soc., 139, 7172–7175, 2017.

[51] A. Sugai, N. Ogawa, and H. Ogawa, “Processing of waste liquid containing radioactive iodine by ion exchange resin column,” 1978.

[52] C. Li, Y. Wei, X. Wang, and X. Yin, “Efficient and rapid adsorption of iodide ion from aqueous solution by porous silica spheres loaded with calcined Mg-Al layered double hydroxide,” J. Taiwan Inst. Chem. Eng., 85, 193–200, 2018.

[53] S. H. Othman, A. M. Elbarbary, G. Rashad, and T. W. Fasih, “Radio-iodide uptake by modified poly (glycidyl methacrylate) as anion exchange resin,” Radiochim. Acta, 105, 75–84, 2017.

[54] T. Nur, W. G. Shim, P. Loganathan, S. Vigneswaran, and J. Kandasamy, “Nitrate removal using Purolite A520E ion exchange resin: batch and fixed-bed column adsorption modelling,” Int. J. Environ. Sci. Technol., 12, 1311–1320, 2015.

[55] H. Li and C. Yang, “Nitrite Removal Using Ion Exchange Resin: Batch vs. Fixed Bed Performance,” Sep. Sci. Technol., 50, 1721–1730, 2015.

[56] M. S. Refat, H. Al. Didamony, K. M. A. El-Nour, and L. El-Zayat, “Synthesis and spectroscopic characterization on the tri-iodide charge transfer complex resulted from the interaction between morpholine as donor and iodine σ-acceptor,” J. Saudi Chem. Soc., 14, 323–330, 2010.

[57] N. Miyajima et al., “A role of charge-transfer complex with iodine in the modification of coal tar pitch,” Carbon N. Y., 38, 1831–1838, 2000.

[58] K. R. Mahmoud, M. S. Refat, T. Sharshar, A. M. A. Adam, and E.-S. A. Manaaa, “Synthesis of amino acid iodine charge transfer complexes in situ methanolic medium: Chemical and physical investigations,” J. Mol. Liq., 222, 1061–1067, 2016.

[59] H. A. Benesi and J. H. Hildebrand, “A Spectrophotometric Investigation of the Interaction of Iodine with Aromatic Hydrocarbons,” J. Am. Chem. Soc., 71, 2703–2707, 1949.

[60] V. Ulagendran, P. Balu, V. Kannappan, R. Kumar, and S. Jayakumar, “Influence of fused aromatic ring on the stability of charge transfer complex between iodine and some five membered heterocyclic molecules through ultrasonic and spectral studies,” J. Mol. Struct., 1141, 213–219, 2017.

[61] B. Camarota, B. Onida, Y. Goto, S. Inagaki, and E. Garrone, “I_2 as a probe for aromatic rings in phenylene-bridged periodic mesoporous organosilica,” in Proceedings of 4th International FEZA Conference, 2008.

[62] J. Milne, “A Raman spectroscopic study of the effect of ion-pairing on the structure of the triiodide and tribromide ions,” Spectrochim. Acta Part A Mol. Spectrosc., 48, 533–542, 1992.

[63] L. Andrews, E. S. Prochaska, and A. Loewenschuss, “Resonance Raman and ultraviolet absorption spectra of the triiodide ion produced by alkali iodide-iodine argon matrix reactions,” Inorg. Chem., 19, 463–465, 1980.

[64] I. Jerman et al., “Ionic conductivity, infrared and Raman spectroscopic studies of 1-methyl-3-propylimidazolium iodide ionic liquid with added iodine,” Electrochim. Acta, 53, 2281–2288, 2008.

[65] J.-X. Lin, J. Liang, J.-F. Feng, B. Karadeniz, J. Lü, and R. Cao, “Iodine uptake and enhanced electrical conductivity in a porous coordination polymer based on cucurbit[6]uril,” Inorg. Chem. Front., 3, 1393–1397, 2016.

[66] L. I. Katzin and E. Gebert, “The Iodide-Iodine-Triiodide Equilibrium and Ion Activity Coefficient Ratios 1,” J. Am. Chem. Soc., 77, 5814–5819, 1955.

Supporting Information

FT-IR spectra

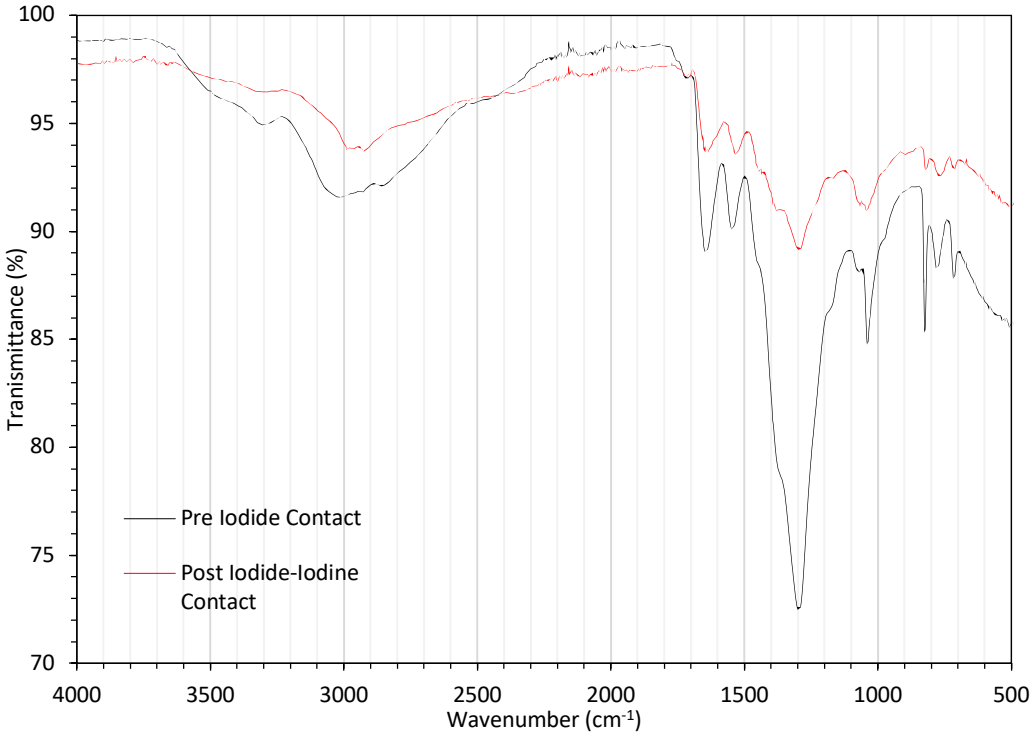

Fig. A.1. Full FT-IR spectra for Purolite S985 both before and after contact with iodide-iodine solution.

Table A.1. FT-IR peak assignment for Purolite S985 before and after contact with iodide-iodine solution.

Pre-Iodide Contact	Post-Iodide/Iodine Contact	Peak Assignment
Peak Wavenumber (cm^{-1})		
3280	3275	N-H st. (2° amine)
3015		sp^2 C-H st. (aromatic)
2875	2975 & 2920	sp^3 C-H st. (alkyl)
~2500 (vague)	Not observed	NH_3^+ symmetric st.
1640 & 1540	1640 &1530	C=C st. (aromatic)
1290	1290	C-O st. (acyl)
1040	1040	C-N st. (aliphatic)
825 & 720	825 & 720	sp^2 C-H bend (aromatic)

Fig. A.2. Full FT-IR spectra for Lewatit A365 both before and after contact with iodide-iodine solution.

Table A.2. Full FT-IR peak assignments for Lewatit A365 both before and after contact with iodide-iodine solution.

Pre-Iodide Contact	**Post-Iodide/Iodine Contact**	**Peak Assignment**
Peak Wavenumber (cm^{-1})		
3280	3280	N-H st. (1° amine)
3050	3040	sp^2 C-H st. (aromatic)
2950	2915 & 2860	sp^3 C-H st. (alkyl)
1530 & 1635	1520 & 1635	C=C st. (aromatic)
1290	1290	C-O st. (acyl)
1035	1035	C-N st. (aliphatic)
825 & 720	825 & 720	sp^2 C-H bend (aromatic)

amide C=O st. would be expected at ~ 1650 cm^{-1}, but cannot be observed.